Supplementary Information (SI) for Physical Chemistry Chemical Physics.

Heterostructured CoFe/Co nanoalloys encapsulated in N-doped carbon as bifunctional oxygen-electrode catalysts for Zn-air batteries

Xiao-Wei Song*[a], Min Lin,[a] Hui Zhao,[a] Ruoxuan Sun[a] and Yebin Guan*[a]

a Anhui Provincial Key Laboratory of Advanced Catalysis and Energy Materials, School of Chemistry and Chemical Engineering, Anqing Normal University, Anqing 246011, China.

E-mail: songxw@aqnu.edu.cn; guanyb@aqnu.edu.cn.

Electrochemical tests

Electrochemical measurements were carried out using a CHI760E workstation equipped with a Pine rotator. A standard three-electrode cell was used to conduct electrochemical experiments, where the working, counter, and reference electrodes were a glassy carbon disk coated with the catalyst, a Pt wire, and an Ag/AgCl electrode, respectively. For the working electrode preparation, typically, 5.0 mg of electrocatalyst was dispersed via ultrasonication in 500 μL of N,N-Dimethylformamide and 500 μL of 0.5 wt% Nafion solution for 2 h to form the catalyst ink. Subsequently, 8 μL of the as-prepared ink was dropped onto the polished glassy carbon disk and allowed to dry completely. For comparison, the benchmark Pt/C (20 wt%) and RuO_2/C (30 wt%) catalysts were dropped onto the electrode surface under the same conditions. The catalyst loading was controlled at 0.203 mg cm^{-2}.

ORR tests

The electrocatalytic activity towards the oxygen reduction reaction (ORR) was evaluated in either 0.1 M KOH or 0.5 M H_2SO_4 solution. First, cyclic voltammetry (CV) measurements were performed in Ar- or O_2-saturated electrolytes at a scan rate of 50 mV s^{-1}. Linear sweep voltammetry (LSV) was conducted in O_2-saturated electrolyte at rotating speeds of 625, 900, 1225, 1600, 2025, and 2500 rpm with a scan rate of 5 mV s^{-1}. The inverse current density (j^{-1}) versus the inverse square root of rotation rate ($\omega^{-1/2}$) plots were fitted with linear curves, and the intercepts were used to calculate the kinetic current density (j_k) and the Tafel slope according to the following equations:

$$\frac{1}{j} = \frac{1}{j_k} + \frac{1}{j_L} = \frac{1}{j_k} + \frac{1}{B\omega^{1/2}} \quad (1)$$

$$\eta = blog(j_k/j_0) \quad (2)$$

where j is the measured current density (mA cm^{-2}), j_k is the kinetic current density (mA cm^{-2}), j_L is the limiting current density (mA cm^{-2}), j_0 is the exchange current density (mA cm^{-2}), ω is the rotating rate (rad s^{-1}), η is the overpotential (η = 1.23 V − E_{RHE}, V), and b is the Tafel slope.

Rotating ring-disk electrode (RRDE) measurements were further employed to assess ORR activity and selectivity. Based on the RRDE data, the electron transfer number (n) and the peroxide yield (HO_2^- in alkaline or H_2O_2 in acid) were calculated using the following equations:

$$n = \frac{4I_d}{I_d + \frac{I_r}{N}} \quad (3)$$

$$H_2O_2(\%) = \frac{200\frac{I_r}{N}}{I_d + \frac{I_r}{N}} \quad (4)$$

where I_d and I_r are the disk and ring current (mA), respectively, and N is the current collection coefficient of the Pt ring (0.37 under the test conditions).

Durability was evaluated via a chronoamperometric measurement at 0.70 V (vs. RHE) for 80000 s in O_2-saturated KOH solution. Accelerated durability tests were conducted by continuous CV cycling between 0.6 and 1.1 V (vs. RHE) at 100 mV s^{-1} for 5000 cycles.

OER tests

The electrocatalytic activity for the oxygen evolution reaction was evaluated in 1 M KOH aqueous solution. LSV curves for all catalysts were recorded at a scan rate of 5 mV s^{-1} and corrected using 85% iR compensation. Electrochemical impedance spectroscopy (EIS) was conducted at 1.62 V (vs. RHE) in the frequency range of 100 kHz to 0.1 Hz. The double-layer capacitance (C_{dl}) was determined from CV performed at scan rates ranging from 20 to 100 mV s^{-1} in the non-

Faradaic potential window of 1.0 – 1.2 V in Ar-saturated 1 M KOH. C_{dl} was calculated as half the slope of the Δj ($j_a - j_c$) versus scan rate plot. Accelerated durability tests were carried out by continuous CV cycling between 1.2 and 1.6 V (vs. RHE) at 100 mV s^{-1} for 2000 cycles.

ZABs measurements

A Zn-air battery (ZAB) was assembled and tested using the CoFe@NC-5 catalyst (loading: 1.5 mg cm^{-2}) supported on carbon paper as the air cathode, a polished Zn plate as the anode, and a mixed electrolyte consisting of 6 M KOH and 0.2 M $Zn(CH_3COO)_2$. For comparison, a control ZAB was assembled using a mixture of commercial Pt/C (20 wt%) and RuO_2 at a 1:1 weight ratio as the air cathode. All tests were conducted under ambient conditions. Polarization curves were recorded using a CHI 760E electrochemical workstation, while galvanostatic charge–discharge tests were performed on a LAND battery testing system. The specific capacity of ZAB was calculated using the following equation:

$$C_{sp} = \frac{i \times t}{\Delta m} \quad (5)$$

where i is the discharge current, t is discharge time, and ∆m represents the mass of zinc plate consumed during the discharge process.

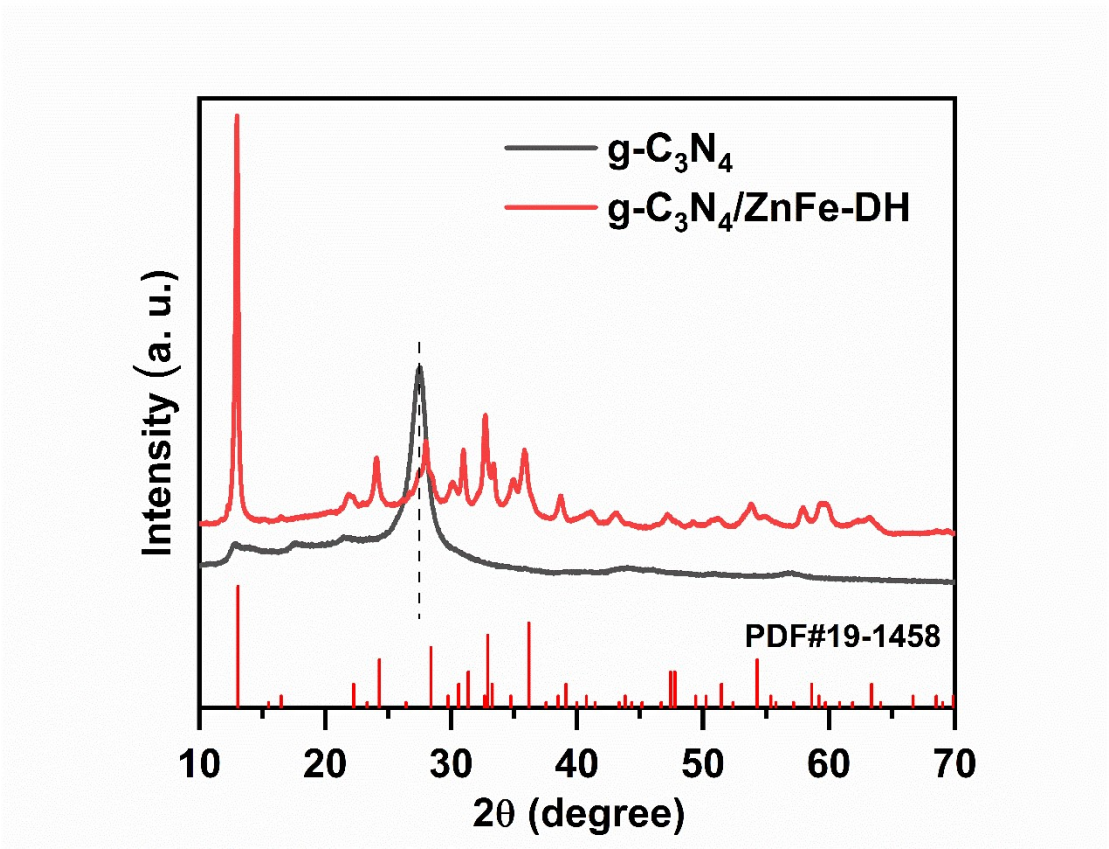

Figure S1. PXRD patterns of g-C_3N_4/ZnFe-DH and pristine g-C_3N_4.

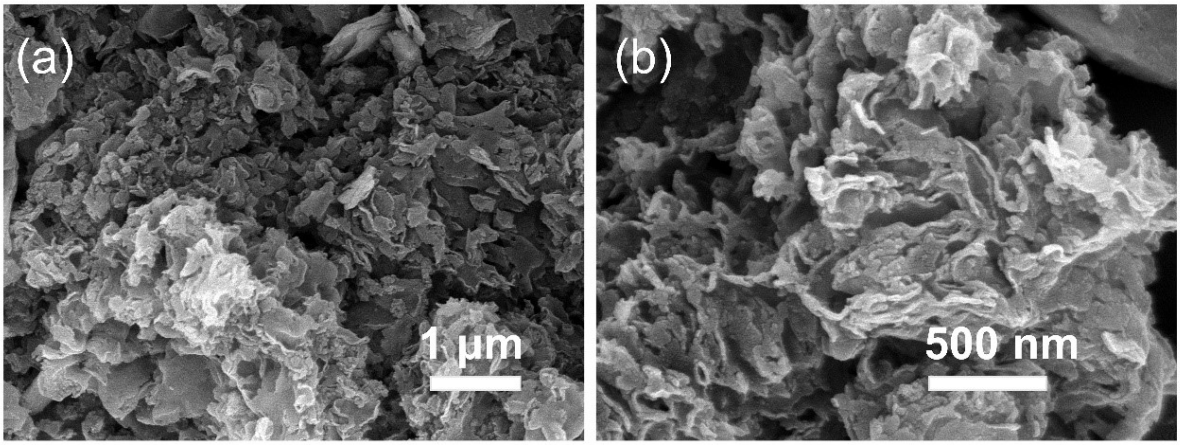

Figure S2. SEM images of g-C_3N_4/ZnFe-DH at different magnifications.

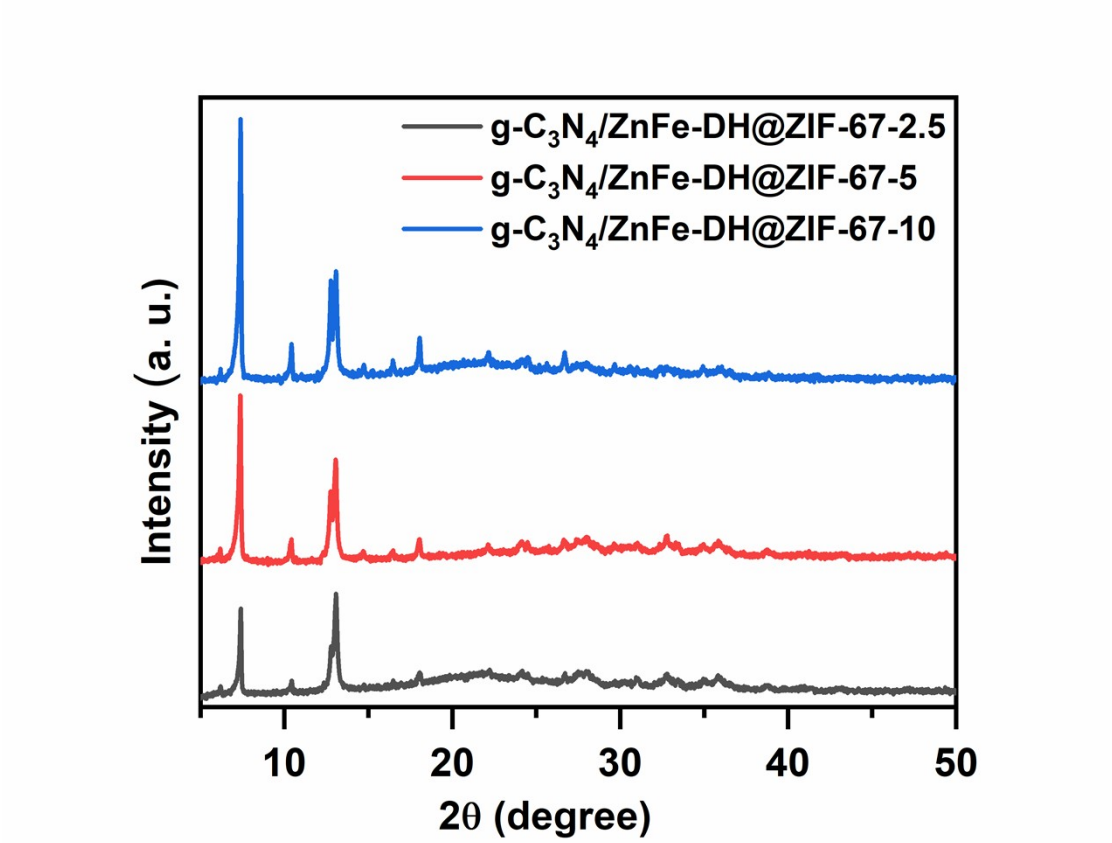

Figure S3. PXRD patterns of g-C_3N_4/ZnFe-DH@ZIF-67-*x* precursors (*x* = 2.5, 5, and 10).

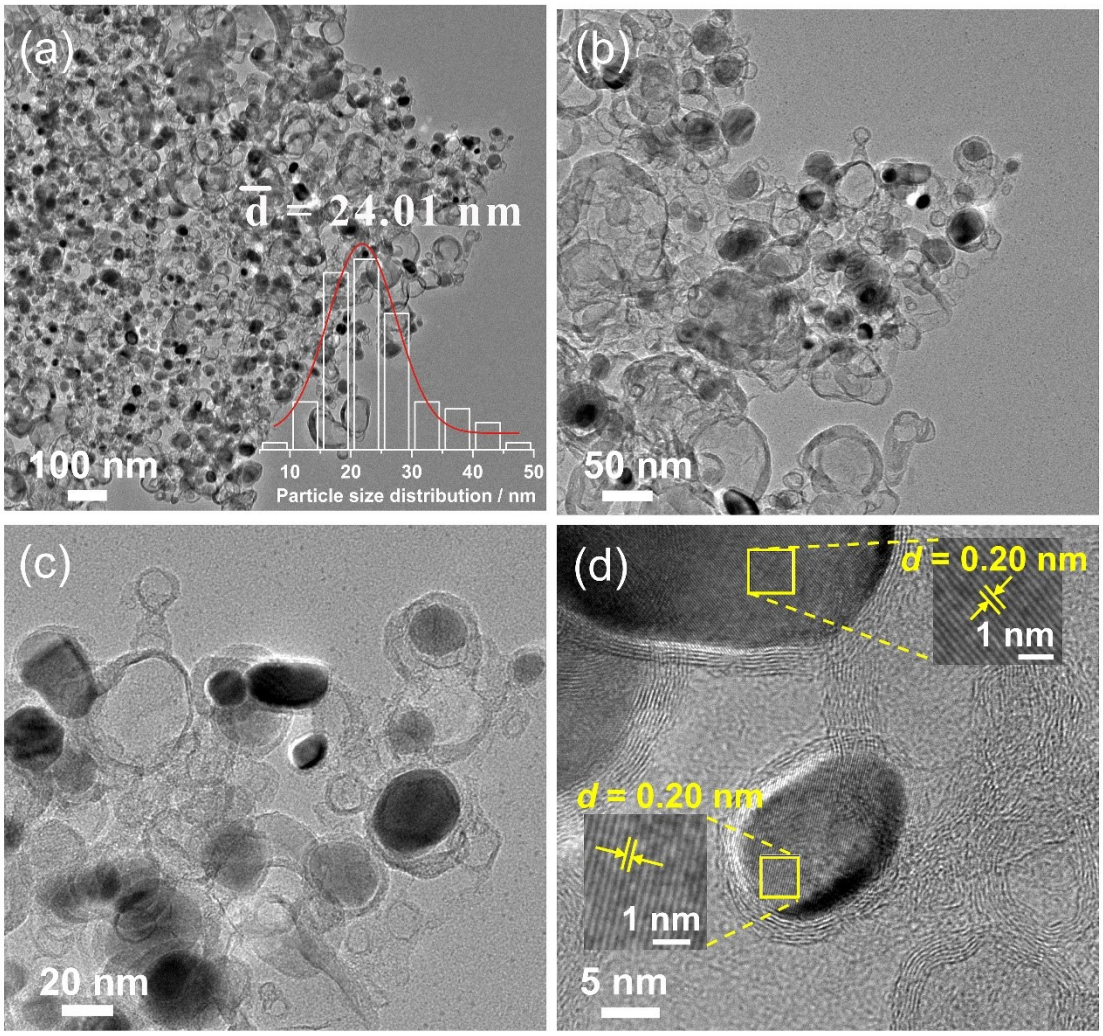

Figure S4. (a-c) TEM and (d) HRTEM images of the CoFe@NC-2.5 sample. Inset in (a) shows the corresponding histogram of the particle size distribution.

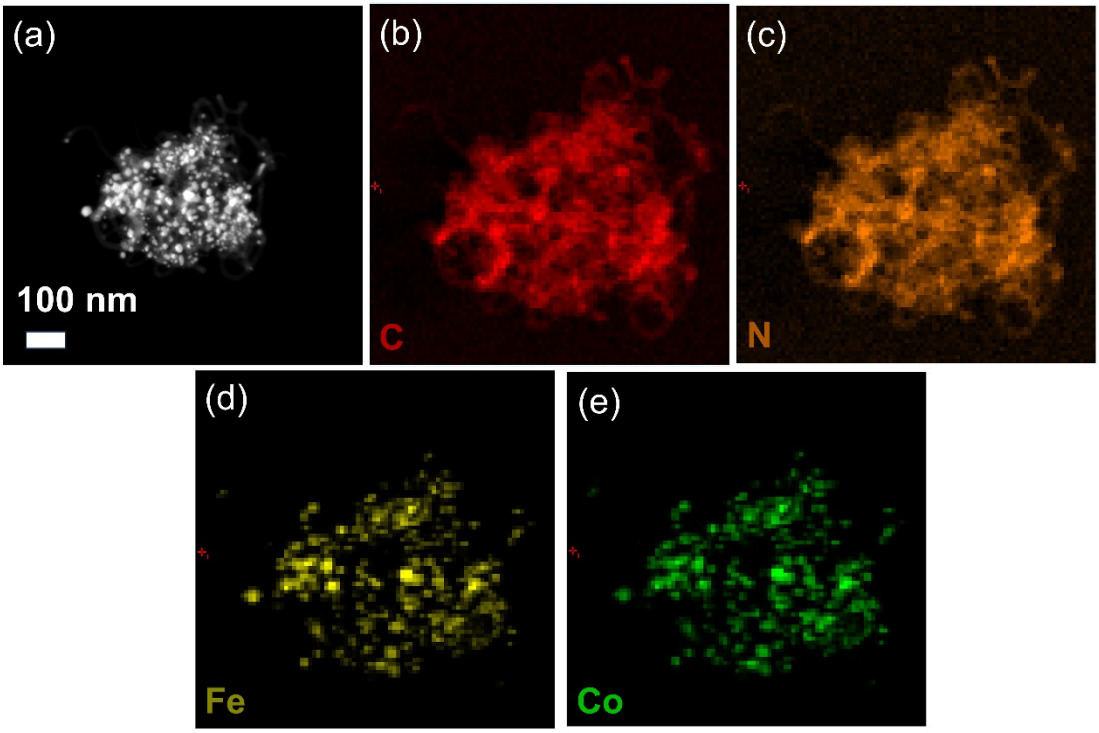

Figure S5. (a) HAADF image of CoFe@NC-5 and elemental mapping images of (b) C, (c) N, (d) Fe, and (e) Co.

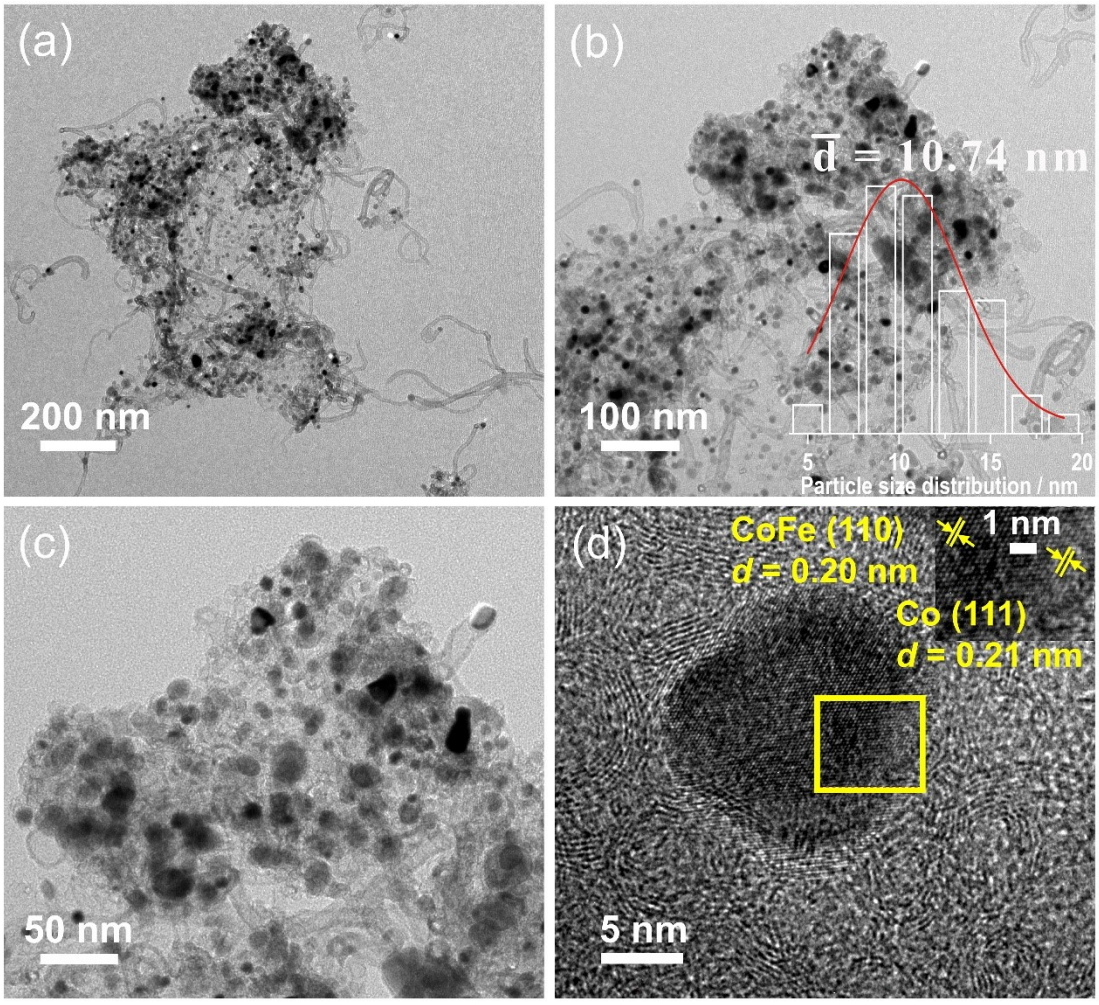

Figure S6. (a-c) TEM and (d) HRTEM images of the CoFe@NC-10 sample. Inset in (b) shows the corresponding histogram of the particle size distribution.

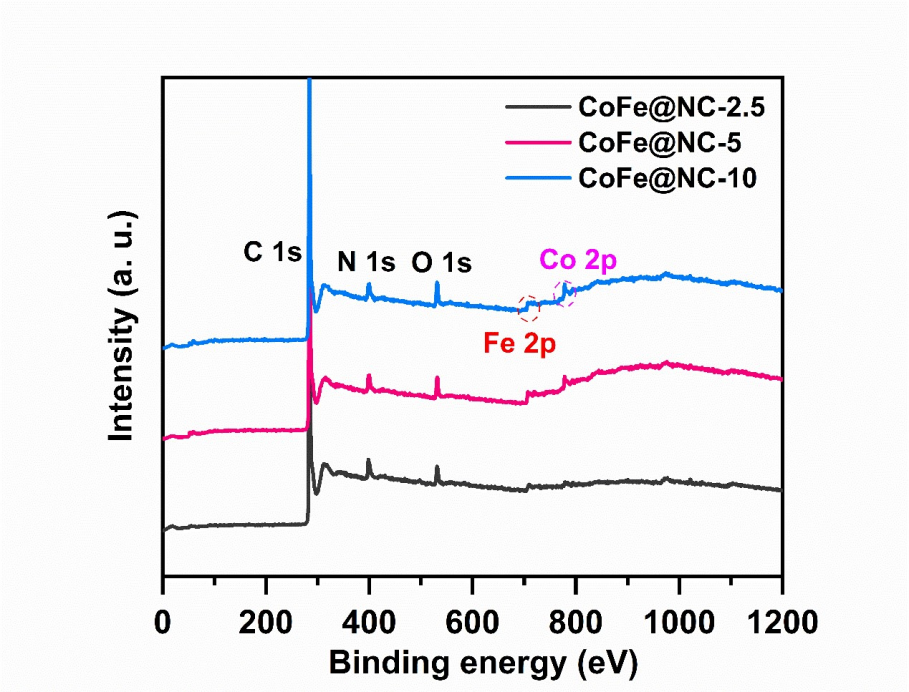

Figure S7. Survey XPS spectra of CoFe@NC-x samples (x = 2.5, 5, and 10).

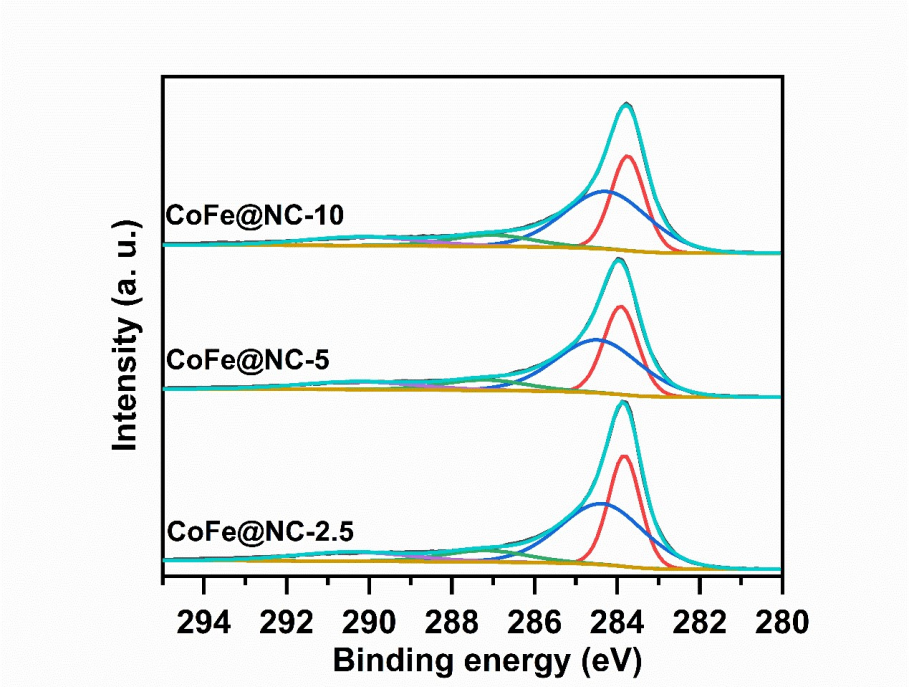

Figure S8. High-resolution C 1s XPS spectra of CoFe@NC-x samples (x = 2.5, 5, and 10).

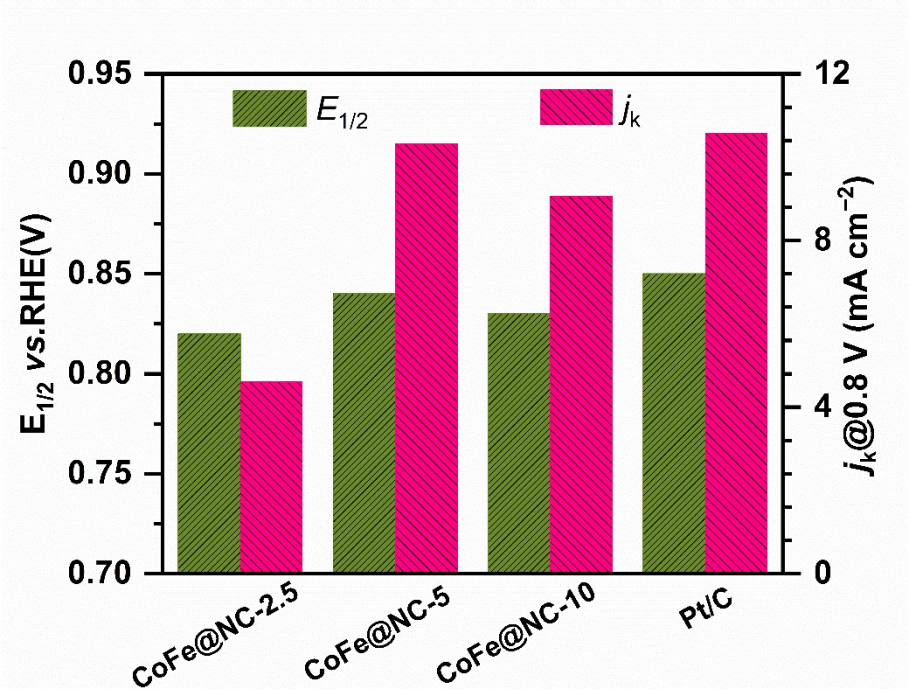

Figure S9. Comparison of ORR half-wave potential ($E_{1/2}$) and kinetic current density at 0.8 V (j_k@0.8 V) for CoFe@NC-x and commercial 20 wt% Pt/C catalysts in 0.1 M KOH solution.

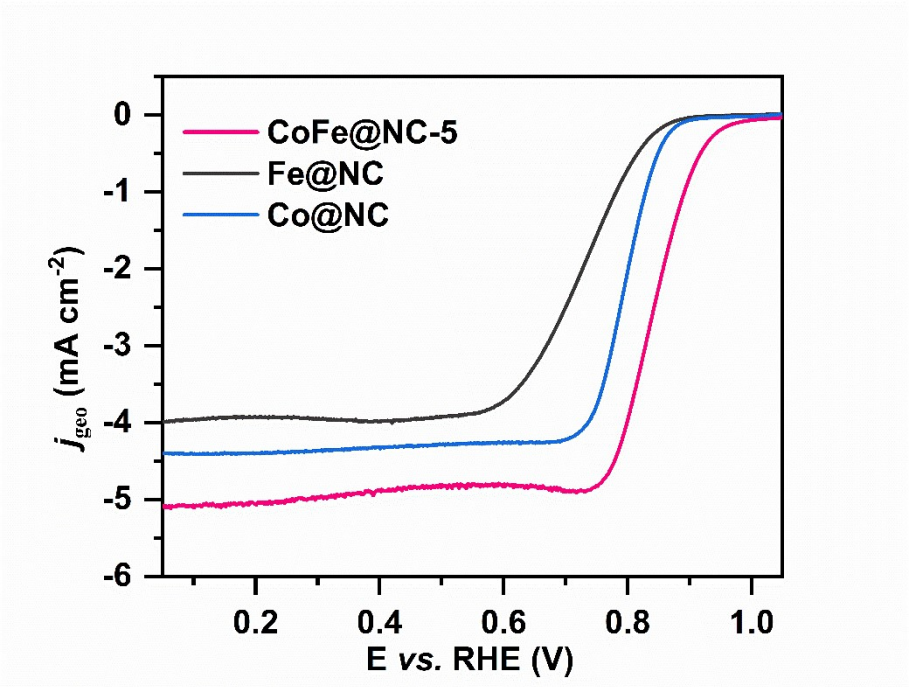

Figure S10. LSV curves of CoFe@NC-5, Fe@NC, and Co@NC catalysts recorded at 1600 rpm with a scan rate of 5 mV s^{-1} in O_2-saturated 0.1 M KOH solution.

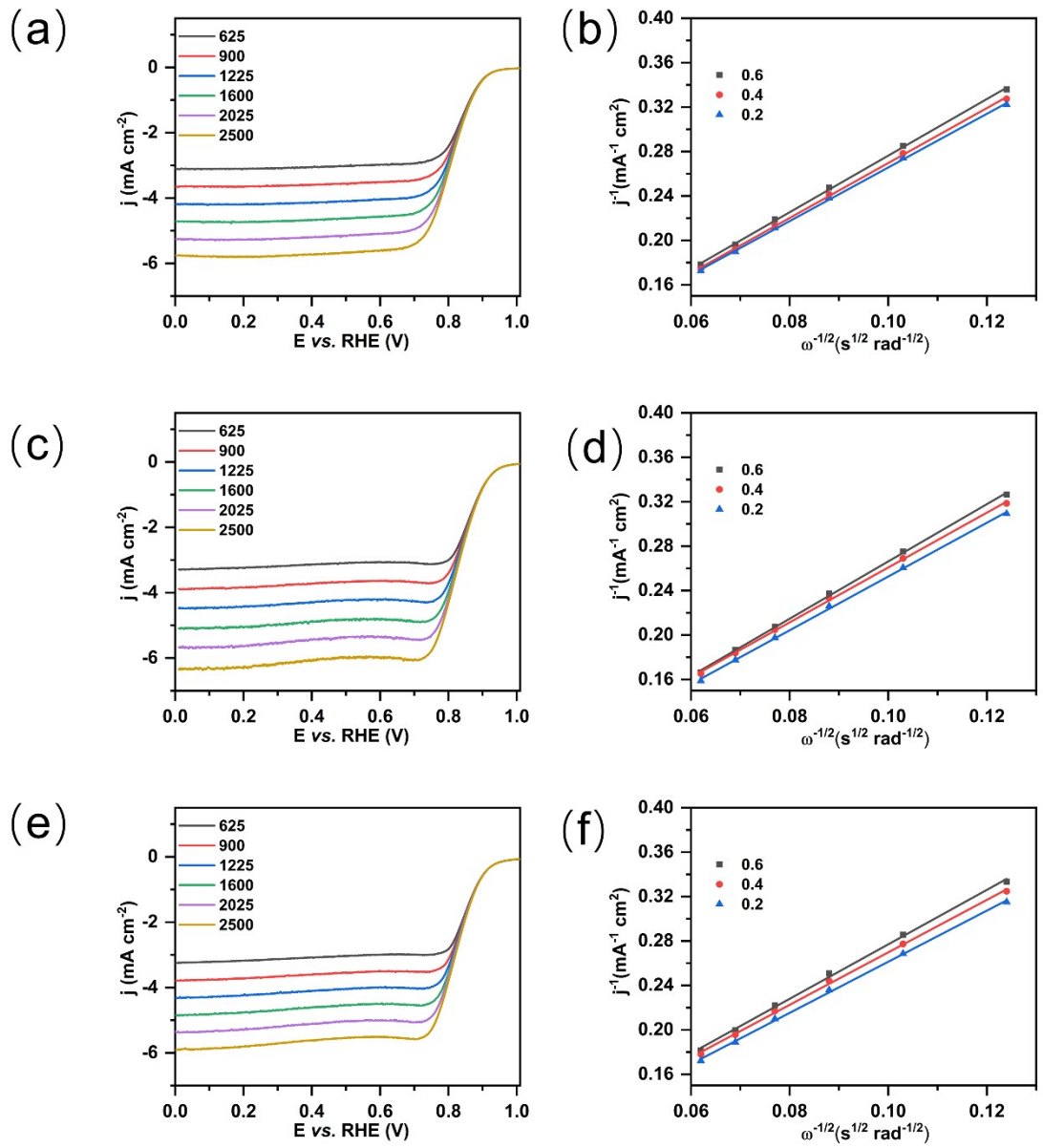

Figure S11. LSV curves of (a) CoFe@NC-2.5, (c) CoFe@NC-5, and (e) CoFe@NC-10 catalysts recorded at different rotation speeds with a scan rate of 5 mV s^{-1} in O_2-saturated 0.1 M KOH solution; corresponding K–L plots calculated from (b) CoFe@NC-2.5, (d) CoFe@NC-5, and (f) CoFe@NC-10 catalysts.

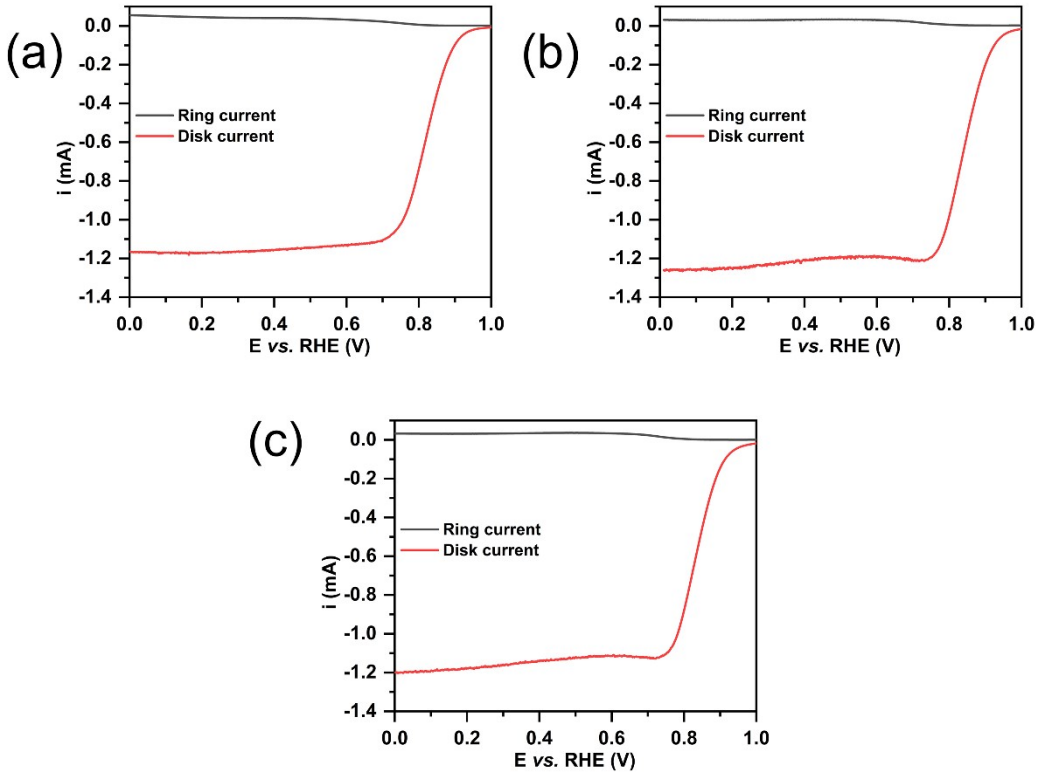

Figure S12. RRDE curves of (a) CoFe@NC-2.5, (b) CoFe@NC-5, and (c) CoFe@NC-10 catalysts recorded at 1600 rpm in O_2-saturated 0.1 M KOH solution.

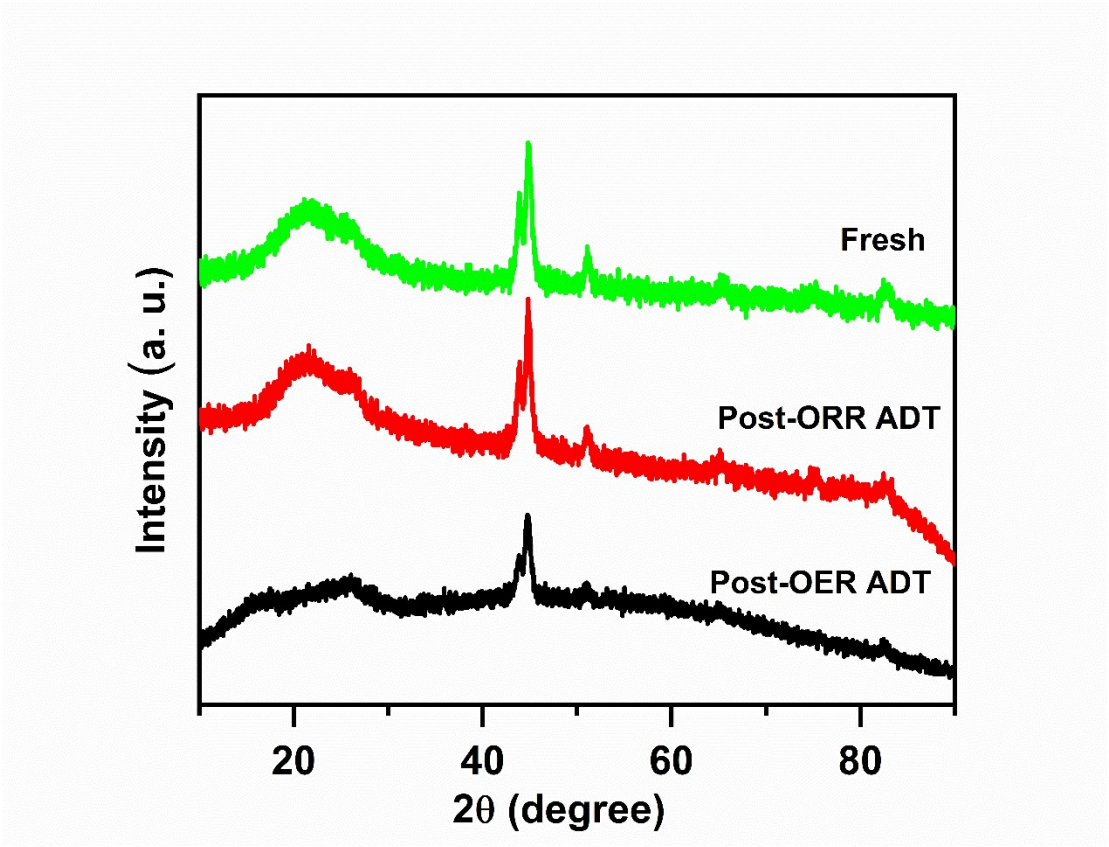

Figure S13. XRD patterns of CoFe@NC-5 before and after accelerated durability tests (ADTs) for ORR and OER.

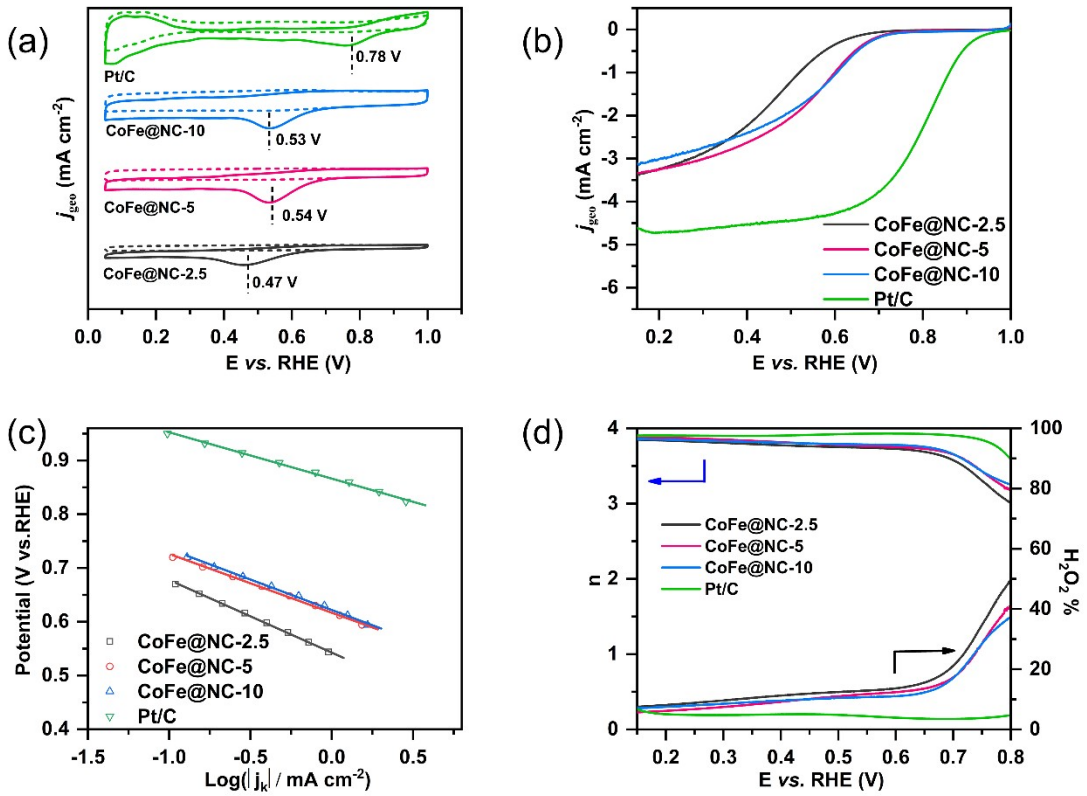

Figure S14. (a) CV curves of CoFe@NC-x and commercial 20 wt% Pt/C catalysts recorded at a scan rate of 50 mV s^{-1} in Ar- and O_2-saturated 0.5 M H_2SO_4 solution; (b) LSV curves of CoFe@NC-x and commercial 20 wt% Pt/C catalysts at 1600 rpm with a scan rate of 5 mV s^{-1} in O_2-saturated 0.5 M H_2SO_4; (c) Tafel plots; (d) electron transfer numbers (*n*) and peroxide (H_2O_2) yields calculated from RRDE data.

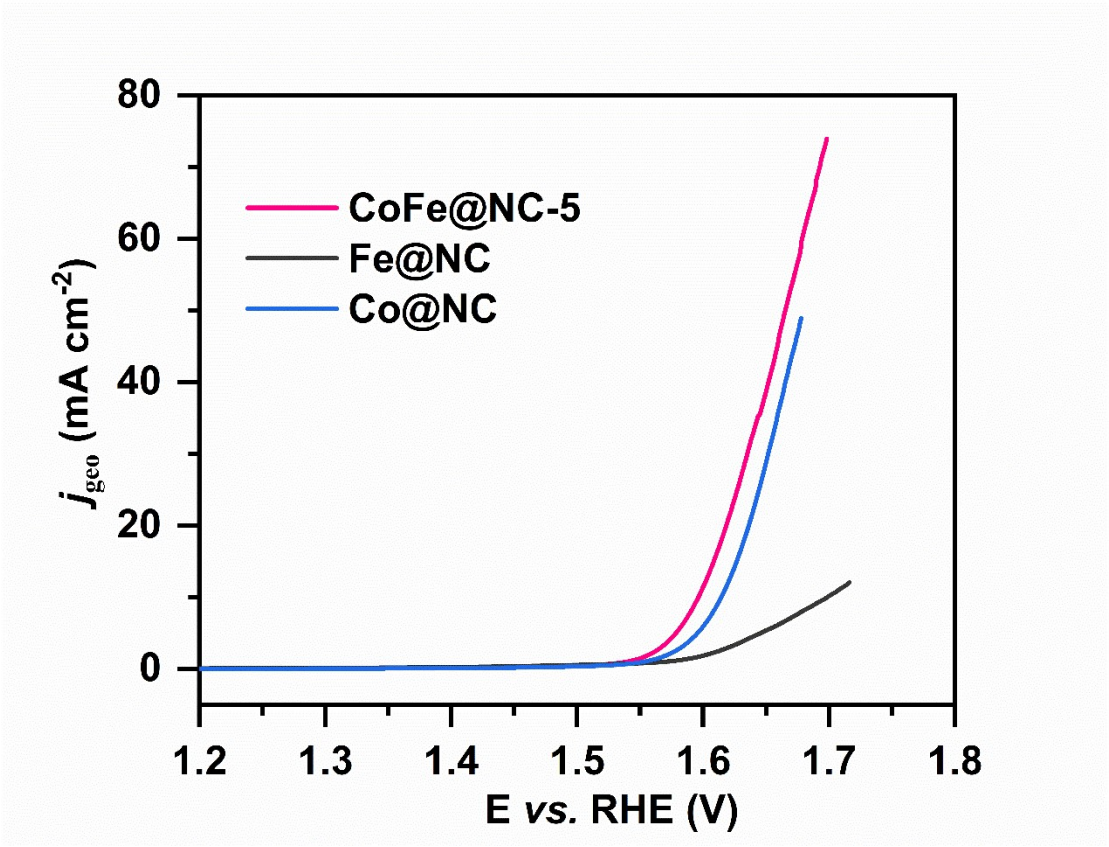

Figure S15. OER polarization curves of CoFe@NC-*5,* Fe@NC, and Co@NC catalysts measured in 1 M KOH with 85% iR compensation.

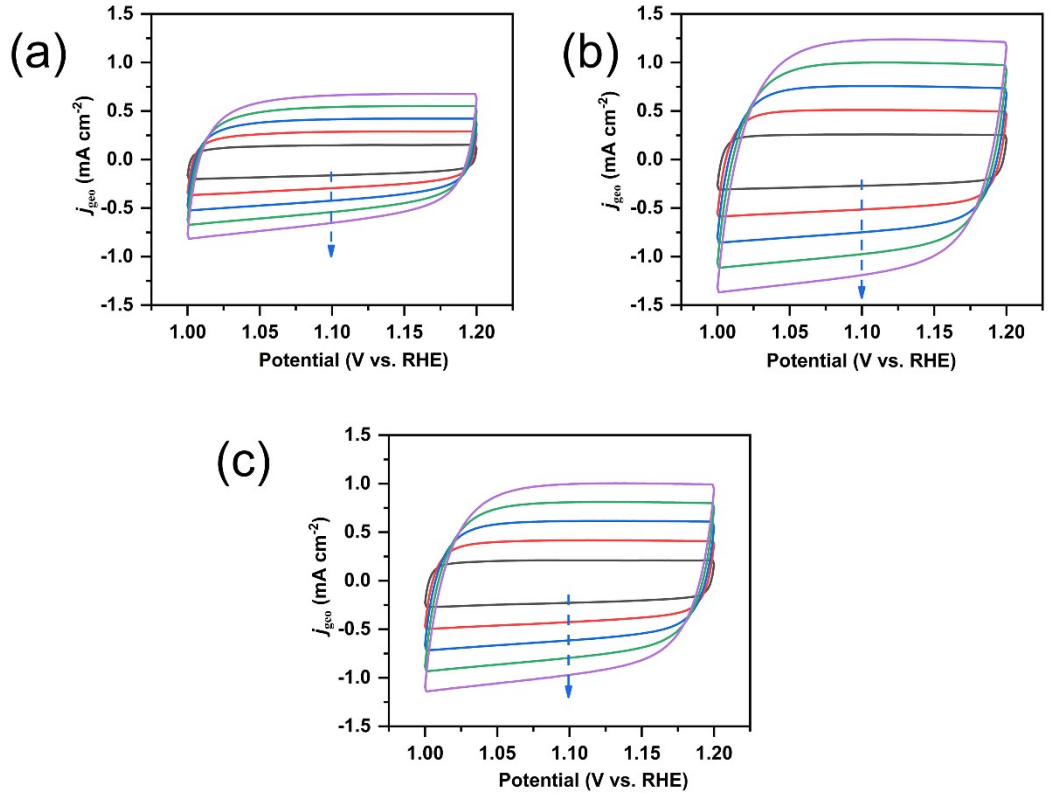

Figure S16. Electrochemical double-layer capacitance (C_{dl}) measurements of (a) CoFe@NC-2.5, (b) CoFe@NC-5, and (c) CoFe@NC-10 catalysts in 1 M KOH, obtained from CV scans at various scan rates ranging from 20 to 100 mV·s^{-1}.

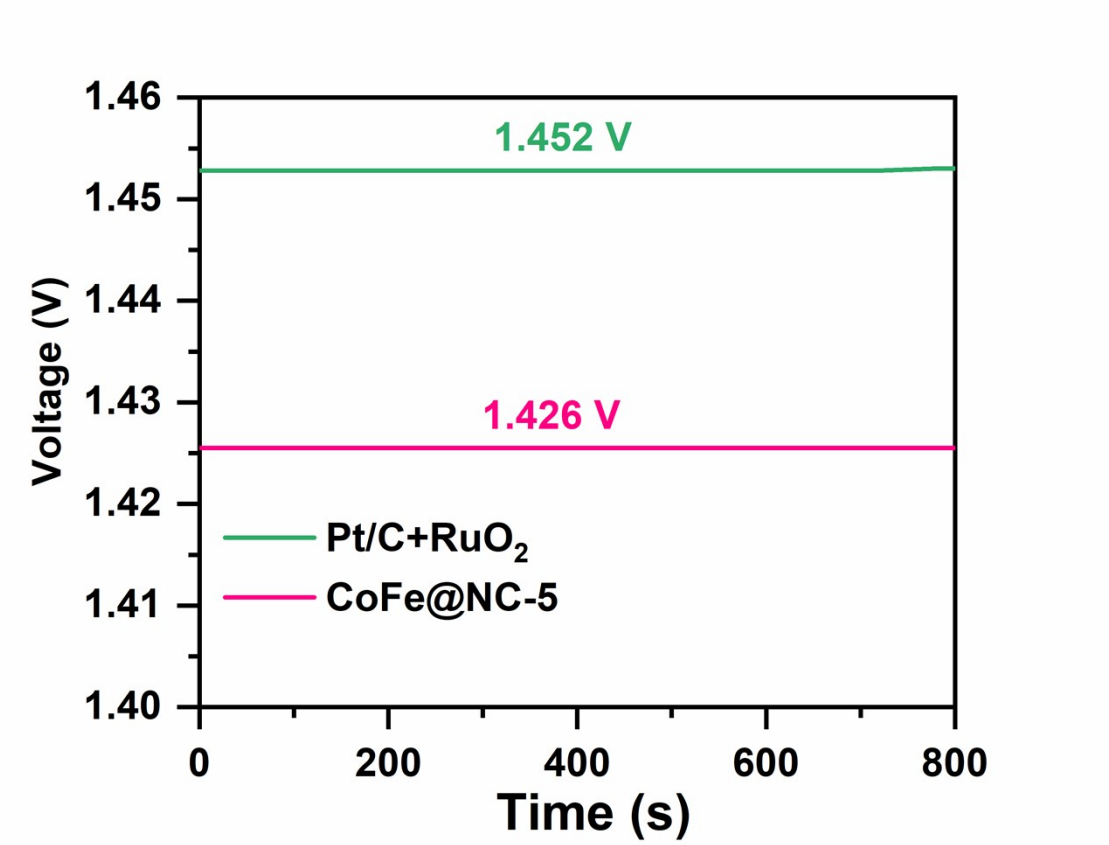

Figure S17. Open-circuit voltage measurements of Zn-air batteries (ZABs) based on CoFe@NC-5 and Pt/C + RuO_2 catalysts.

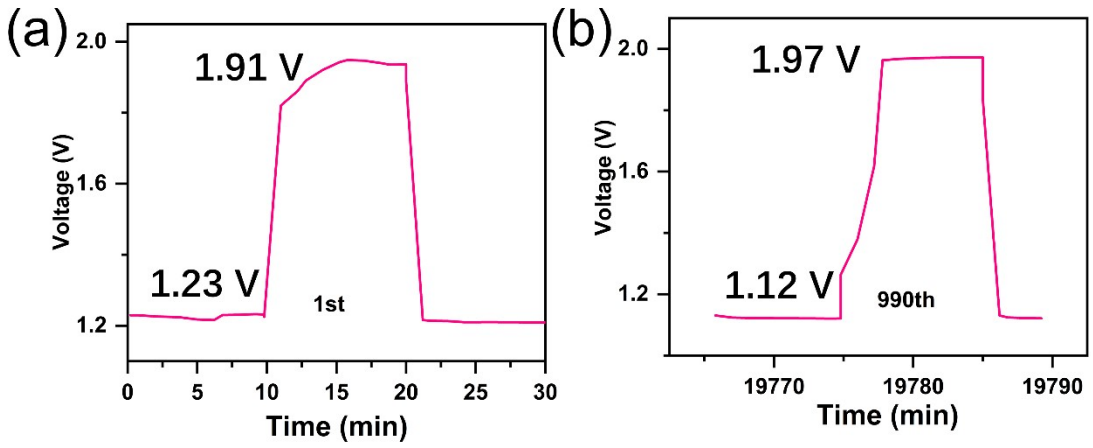

Figure S18. Galvanostatic charge-discharge curves of CoFe@NC-5-based ZAB at 10 mA·cm^{-2} (a) the 1st cycle and (b) the 990th cycle.

Table S1. Fe and Co mass percentages in CoFe@NC-x samples determined by ICP-OES analysis.

samples	Fe (wt%)	Co (wt%)	Fe Relative (%) [a]	Co Relative (%) [b]
CoFe@NC-2.5	21.66	5.88	78.65	21.35
CoFe@NC-5	23.84	13.40	64.02	35.98
CoFe@NC-10	16.38	17.13	48.88	51.12

a: Fe Relative (%) = Fe (wt%)/(Fe (wt%) + Co (wt%))
a: Co Relative (%) = Co (wt%)/(Fe (wt%) + Co (wt%))

Table S2. Surface atomic composition of the as-prepared CoFe@NC-x samples obtained from XPS analysis.

samples	C 1s (at. %)	O 1s (at. %)	N 1s (at. %)	Co 2p (at. %)	Fe 2p (at. %)
CoFe@NC-2.5	90.12	3.88	5.2	0.29	0.51
CoFe@NC-5	89.27	3.95	5.26	0.66	0.86
CoFe@NC-10	89.02	4.07	5.5	0.68	0.73

Table S3. Relative contents of different types of nitrogen species in CoFe@NC-x samples derived from XPS analysis.

Samples	CoFe@NC-2.5 (%)	CoFe@NC-5 (%)	CoFe@NC-10 (%)
Pyridinic N	37.80	29.03	32.31
Co(Fe)-N_x	10.41	14.44	10.70
Pyrrolic N	33.74	37.93	37.15
Graphitic N	10.98	15.00	10.88
Oxidized N	7.07	3.60	8.96

Table S4. ORR parameters of CoFe@NC-x electrocatalysts (x = 2.5, 5, and 10) and commercial 20 wt% Pt/C in both alkaline and acidic media.

Electrocatalysts	0.1 M KOH					
	E_{onset} (V *vs*. RHE)	$E_{1/2}$ (V)	j_k @ 0.8 V (mA cm^{-2})	Tafel slopes (mV dec^{-1})	*n*	H_2O_2%
CoFe@NC-2.5	0.94	0.82	−4.62	77	3.69	15.45
CoFe@NC-5	0.98	0.84	−10.32	66	3.81	9.65
CoFe@NC-10	0.98	0.83	−9.06	72	3.73	13.35
20% Pt/C	1.00	0.85	−10.58	66	3.97	1.27
	0.5 M H_2SO_4					
	E_{onset} (V *vs*. RHE)	$E_{1/2}$ (V)	j_k @ 0.7 V (mA cm^{-2})	Tafel slopes (mV dec^{-1})	*n*	H_2O_2%
CoFe@NC-2.5	0.67	0.45	- 0.12	135	3.71	14.12
CoFe@NC-5	0.72	0.54	- 0.17	109	3.77	11.75
CoFe@NC-10	0.72	0.53	- 0.19	113	3.76	12.87
20% Pt/C	0.95	0.80	-12.85	86	3.90	4.17

Table S5. Comparison of ORR/OER and Zn-air battery performance between this work and previous reports on carbon-encapsulated FeCo-based heterostructured alloy electrocatalysts in alkaline media.

Electrocatalysts	ORR		OER	Bifunctional activity	Zn-air battery		Refs
	$E_{1/2}$ [a] (V)	j_L (mA cm^{-2})	$E_{j=10}$ [b] (V)	$\Delta E=E_{j=10}-E_{1/2}$ (V)	Open circuit voltage (V)	Power density (mW cm^{-2})	
CoFe@Fe_3N-CNT	0.936	5.12	1.56	0.624	1.534	173.6	[1]
CoFe-Co@PNC-12	0.887	6.0	1.55	0.663	1.45	152.8	[2]
$Co_{0.7}Fe_{0.3}$@$NC_{2:1}$-800	0.827	4.9	1.544	0.717	1.449	85.7	[3]
Co/CoFe@NC	0.84	6.8	1.54	0.7	1.49	146.6	[4]
$Co_{5.47}N/Co_3Fe_7$/NC	0.89	5.73	1.609	0.719	1.502	264	[5]
FeCo@Co/N-C-8	0.87	5.73	1.542	0.672	1.52	148	[6]
CoFe-CoC_X@NCNT-2	0.89	3.8	1.63	0.74	1.42	175	[7]
CoFe-Co_3C@NCNTs-20	0.934	5.0	1.55	0.616	1.505	209	[8]
Co-CoFe@NRPC-90	0.885	6.15	1.55	0.665	1.507	281	[9]
CoFe@NCNTs	0.84	5.0	1.482	0.642	1.60	158.4	[10]
CoFe-$Co_{5.47}N$@NC	0.79	5.4	1.634	0.844	1.46	178	[11]
FeCo/N-CNFs	0.88	5.2	1.58	0.7	1.445	356.2	[12]
FeCo/Co-N-C	0.86	5.42	1.61	0.75	1.53	188	[13]

Co/Co_7Fe_3@PNCC	0.899	5.5	1.525	0.626	1.534	211.8	[14]
Co/Co_3Fe_7@NCNTs-800	0.89	4.4	1.51	0.62	1.52	165	[15]
$CoFe_{0.08}$@NCS	0.8	5.4	1.513	0.713	1.425	157	[16]
CoFe@NC-5	0.84	5.10	1.597	0.757	1.426	363.7	This work

a: $E_{1/2}$, half-wave potential in ORR

b: $E_{j = 10}$, the operating potential at 10 mA cm^{-2} in OER

References

1. Y.-R. Hao, H. Xue, L. Lv, J. Sun, N. Guo, T. Song, H. Dong, J. Zhang and Q. Wang, *Appl. Catal. B: Environ.*, 2021, **295**, 120314.
2. Z. Lei, Y. Tan, Z. Zhang, W. Wu, N. Cheng, R. Chen, S. Mu and X. Sun, *Nano Res.*, 2021, **14**, 868-878.
3. L. Long, H. Liu, J. Jia, Y. Zhang and S. Dong, *Nanoscale*, 2021, **13**, 2609-2617.
4. Y. Niu, X. Teng, S. Gong, M. Xu, S.-G. Sun and Z. Chen, *Nano-Micro Letters*, 2021, **13**, 126.
5. L. Li, J. Chen, S. Wang, Y. Huang and D. Cao, *Appl. Surf. Sci.*, 2022, **582**, 152375.
6. L. Song, J. Zhang, S. Sarkar, C. Zhao, Z. Wang, C. Huang, L. Yan and Y. Zhao, *Chem. Eng. J.*, 2022, **433**, 133686.
7. J. Sun, N. Guo, T. Song, Y.-R. Hao, J. Sun, H. Xue and Q. Wang, *Advanced Powder Materials*, 2022, **1**, 100023.
8. X. Meng, J. Xie, J. Liu, B. Liu, R. Wang, P. Gu, F. Ma, X. Wang and J. Zou, *Chem. Eng. J.*, 2023, **459**, 141591.
9. H.-H. Yang, X.-R. Qian, N. Zhang, X.-T. Jia, Z.-Y. Wen, X.-B. Chen and M.-J. Zhou, *Rare Metals*, 2023, **42**, 3766-3779.
10. D. Ye, Y. Shen, H. Mao, Y. Liang, Q. Gao, S. Yang, S. Zhang, X. Cai and Y. Fang, *Chem. Eng. J.*, 2023, **464**, 142601.
11. J. Zhang, J. Liu, B. Liu, X. Lin and Y. Qin, *Chem. Eng. Sci.*, 2023, **280**, 119049.
12. J. Zhang, Y. Zhang, C. Xu, Y. Li, G. Ni, P. Huo, V. Balasubramani, Z. Li and B. Liu, *J. Alloys Compd.*, 2023, **948**, 169721.
13. J. Zhong, Z. Zhu, Q. Xu, L. Peng, K. Luo and D. Yuan, *Energy & Fuels*, 2023, **37**, 13489-13497.
14. Y. Lian, T. Yu, Y. Qu, C. Yuan, Z.-H. Lu and M. Guo, *Industrial & Engineering Chemistry Research*, 2024, **63**, 1369-1379.
15. X. Liu, S. Huo, X. Xu, X. Wang, W. Zhang, Y. Chen, C. Wang, JiahaoXie, X. Liu, H. Chang and J. Zou, *J. Colloid Interf. Sci.*, 2024, **666**, 296-306.
16. J. Chen, Y. Zhuang, Y. Qiao, Y. Zhang, A. Yuan and H. Zhou, *International Journal of Minerals, Metallurgy and Materials*, 2025, **32**, 476-487.